Laser damage resistant anti-reflection microstructures for mid-infrared metal-ion doped ZnSe gain media.

Douglas S. Hobbs*, Bruce D. MacLeod, Ernest Sabatino III
TelAztec LLC, 15 A Street, Burlington, MA, USA 01803-3404
and
Sergey B. Mirov, Dmitri V. Martyshkin
IPG Photonics Corporation, 1500 First Avenue North, Birmingham, AL USA 35203

ABSTRACT

Power scaling of mid-infrared laser systems based on chromium and iron doped zinc selenide (ZnSe) and zinc sulfide (ZnS) crystals is being advanced through the integration of surface relief anti-reflection microstructures (ARMs) etched directly in the facets of the laser gain media. In this study, a new ARMs texture fabrication process is demonstrated for polycrystalline ZnSe and ZnS material that results in a significant increase in pulsed laser damage resistance combined with an average reflection loss of less than 0.5% over the wavelength range of 1.9-3.0µm. The process was utilized to fabricate ARMs in chromium-doped zinc selenide (Cr^{2+}:ZnSe) materials supplied by IPG Photonics and standardized pulsed laser induced damage threshold (LiDT) measurements at a wavelength of 2.09µm were made using the commercial testing services of Spica Technologies. It was found that the pulsed LiDT of ARMs etched in ZnSe and Cr^{2+}:ZnSe can match or even exceed the level of a well-polished surface, a survivability that is many times higher than an equivalent performance broad-band thin-film AR coating. The results also indicate that the ARMs plasma etch process may find use as a post-polish damage mitigation technique similar to the chemical immersion used to double the damage resistance of fused silica optics. ARMs etched in Cr^{2+}:ZnSe were also evaluated by IPG Photonics for survivability under continuous wave (CW) laser operation at a pump laser wavelength of 1.94µm. Catastrophic damage occurred between power levels of 400-500 kilowatt per square centimeter for both as polished and ARMs textured samples indicating no reduction in CW damage resistance attributable to surface effects.

Keywords: Mid-IR Lasers, Antireflection, AR, Motheye, Microstructures, LIDT, Thin-Film AR Coatings, Cr:ZnSe

1.0 INTRODUCTION

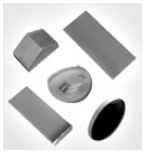

Solid state lasers based on optical excitation of chromium ions diffused within II-VI semiconductor material hosts such as zinc selenide (ZnSe) and zinc sulfide (ZnS), are proving to be attractive sources of high power tunable mid-infrared (mid-IR) light[1-7]. Cr^{2+}:ZnSe and Cr^{2+}:ZnS laser materials are typically produced by conventional vacuum diffusion of chromium into pre-formed polycrystalline slabs, windows, or lenses such as those shown on the right. Chromium ions absorb short wavelength IR photons within the 1.5-2.0 µm wavelength range, and emit photons at longer wavelengths within the 2.1-3.4 µm range. The optical conversion efficiency is very high for Cr^{2+}:ZnSe material, allowing a laser constructed in the conventional manner to power scale using multiple high power lasers as pump sources. Typical solid-state laser pump sources are quite sensitive to back reflections that can de-stabilize a laser resonator and even damage laser cavity components. In particular, the input facet of the Cr^{2+}:ZnSe gain material must tolerate a high pump light flux, and must pass a wide range of wavelengths in tunable configurations, requirements that are difficult to meet using conventional thin-film anti-reflection (AR) coatings due to poor adhesion to II-VI materials and water vapor absorption. In fact, to avoid using low survivability coatings in Cr^{2+}:ZnSe mid-IR laser systems, many researchers will use a cavity configuration that includes Brewster angle illumination. In the case of Cr^{2+}:ZnSe, Brewster's angle is nearly 68 degrees. Such a large cavity asymmetry aggravates thermal lensing problems, requires complex aspheric components, and forces the use of polarized light which cuts the output power potential in half.

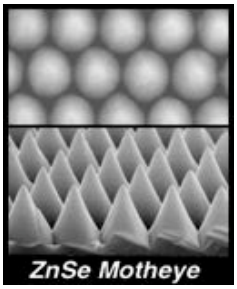

To utilize a simpler, power scalable in-line laser cavity configuration, surface relief AR microstructures (ARMs), like those shown formed in ZnSe in the scanning electron micrographs (SEMs) on the right, can be etched directly in the Cr^{2+}:ZnSe crystal facets, providing the wide bandwidth and high damage resistance required for further power scaling. In an Air Force Research Laboratory (AFRL) sponsored project, the utility of ARMs textures was demonstrated through prototype fabrication and standardized laser induced damage threshold (LiDT) testing. Also in collaboration with IPG Photonics, an initial test was made of the continuous wave (CW) damage threshold of ARMs treated Cr^{2+}:ZnSe crystals.

* dshobbs@telaztec.com; phone 1 781 229-9905; www.telaztec.com

Laser-Induced Damage in Optical Materials: 2012, edited by Gregory J. Exarhos, Vitaly E. Gruzdev, Joseph A. Menapace, Detlev Ristau, M J Soileau, Proc. of SPIE Vol. 8530
85300P · © 2012 SPIE · CCC code: 0277-786/12/$18 · doi: 10.1117/12.2016402

2.0 BACKGROUND: AR MICROSTRUCTURE TECHNOLOGY

If the surface of an optic is broken by a series of depressions or protrusions with a size and spacing that is everywhere smaller than the wavelength of the light to be manipulated by the optic, then light losses due to scattering or diffraction will not occur and a gradual refractive index change will be created. So long as this gradient index effect is sufficiently slow, a wide range of light wavelengths will pass without the typical Fresnel reflection loss from an abrupt index change at a flat interface. ARMs textures are optimized to yield this gradient index function, and are commonly known as *Motheye* when the sub-wavelength-sized features are arrayed in a regular or periodic array[8]. Being fabricated in the surface of the bulk optic material, Motheye structures have been shown to be superior in environmental durability, with increased radiation, thermal shock, and impact resistance, yielding long-term reliability[9-14]. Recent demonstrations have indicated a superior laser power handling capability for ARMs compared to thin film AR coatings[15-21].

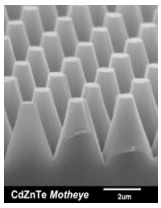

Motheye ARMs have been demonstrated in many materials that transmit light with wavelengths ranging from the ultraviolet (UV) through the long wave infrared (LWIR). As an example of the extreme performance demonstrated by ARMs, a Motheye cone-array (seen in the SEM on the right) fabricated in a cadmium zinc telluride (CdZnTe) substrate designed for sensors collecting LWIR light, was measured by the National Institute of Standards and Technology (NIST) to exhibit an average reflection loss of 0.2% over the 8-12µm wavelength band (down from nearly 21% for an untreated CdZnTe surface), a level unattainable with available thin film AR coating materials[12].

Figure 1 shows overhead and elevation SEM images of Motheye ARMs that have been fabricated in different optical materials. From left to right- the image strip shows Motheye ARMs in silicon carbide (SiC), silicon, arsenic sulfide (As_2S_3), and ZBLAN (ZrF_4-BaF_2-LaF_3-AlF_3-NaF). Note that the As_2S_3 and ZBLAN ARMs are embossed prints from the ARMs-treated silicon substrate that served as a master template. The concept of embossing ARMs directly in the end facets of chalcogenide and fluoride fibers is being developed to provide enhanced transmission and an increased power handling capacity for mid-IR laser delivery systems used in IR countermeasure and medical laser applications[20]. Replication through embossing is an attractive option for applying ARMs to mid-IR transmitting glasses due to the significant fabrication cost savings expected.

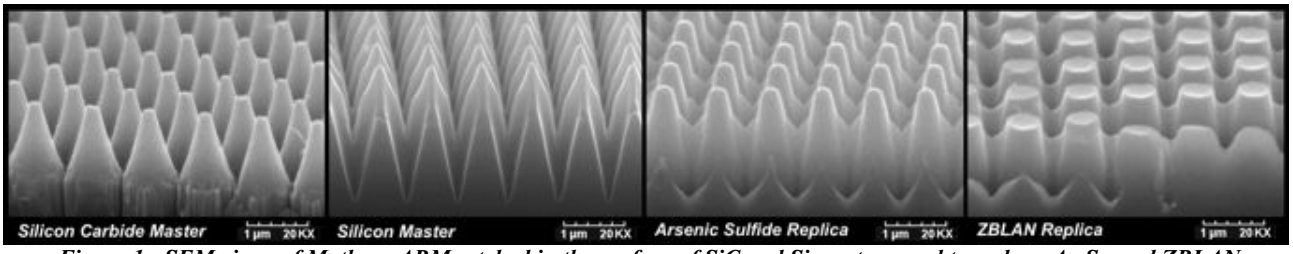

Figure 1: SEM views of Motheye ARMs etched in the surface of SiC and Si masters used to emboss As_2S_3, and ZBLAN.

2.1 ARMs TEXTURE DESIGN MODELING

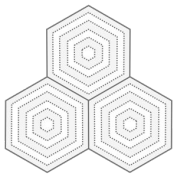

Computer simulations based on rigorous coupled wave theory (RCWA) are used to design and guide the fabrication of ARMs textures, as well as textures that impart filtering, polarizing, and high reflector (HR) functions. The software allows the propagation of light through a user defined three-dimensional surface texture composed of multiple structured and uniform materials. By solving Maxwell's equations at each material interface, the model predicts the spectral reflectance and transmittance, accounting for arbitrary polarization states and light incident angles. Measured data for the optical constants of a library of materials is included and regularly updated and augmented. Model predictions have proven to be a good match to measured AR microstructure, polarizer, and HR microstructure prototype performance[10,18].

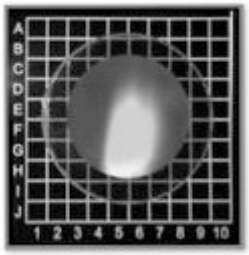

To illustrate the utility of modeling as an accurate predictor of the performance of fabricated ARMs textures, Figure 2 shows SEM images of a Motheye ARMs textured ZnSe window surface that exhibits the measured mid-IR transmission given in Figure 3 (black curve with diamond markers) compared with the transmission of ARMs textures simulated by the modeling software. The cone structures, fabricated in one surface of multiple 1-inch round, 2mm thick ZnSe windows like that shown on the right, are just over 1µm tall and arrayed on a hexagonal grid with a spacing of 0.75µm. Square based pyramids arrayed on a 0.8µm pitch that are 1.0 µm tall with a linear taper and a base width over 95% of the grid pitch (high fill factor), were input to the calculation resulting in the light gray dot-dash curve. An FTIR

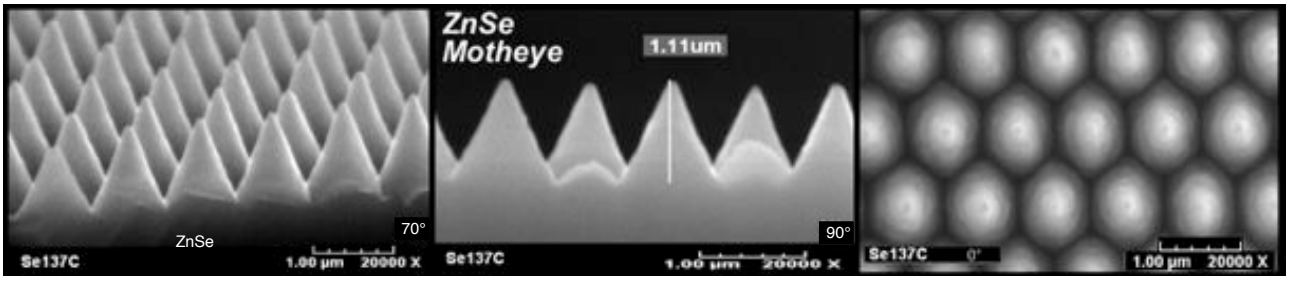

Figure 2: Elevation (70°), profile (90°), and overhead (0°) SEM images of 1.1µm deep ZnSe Motheye structures.

spectrophotometer (Thermo Nicolet Magna 550 with upgraded interferometer block, extended range beam-splitter, and data acquisition software) was used to measure the spectral transmission through the ZnSe windows over the infrared wavelength range of 1.7 to 22μm. Both the measured data and the model results show maximum transmission over the wavelength range of 1.95 to 2.5µm (as compared to the theoretical maximum plotted as the light gray dotted curve at 82.4%) with the measured data decreasing more rapidly than the model for longer wavelengths. (Note that water vapor absorption lines between 2.55 and 2.85µm have been eliminated from the measured data along with CO_2 absorption centered at 2.15µm). Predictions for two other types of ARMs textures in ZnSe are shown in the figure as the dashed black curve indicating the Hybrid ARMs design that consists of an array of isolated and truncated (steep sidewall) pyramids 0.8µm tall, and an array of square posts 0.37µm tall simulating the binary effective index SWS ARMs texture (dotted gray curve). For single wavelength applications the more easily fabricated SWS texture is preferred, but for tunable laser applications needing broader band performance, Motheye or Hybrid ARMs textures are the best choice.

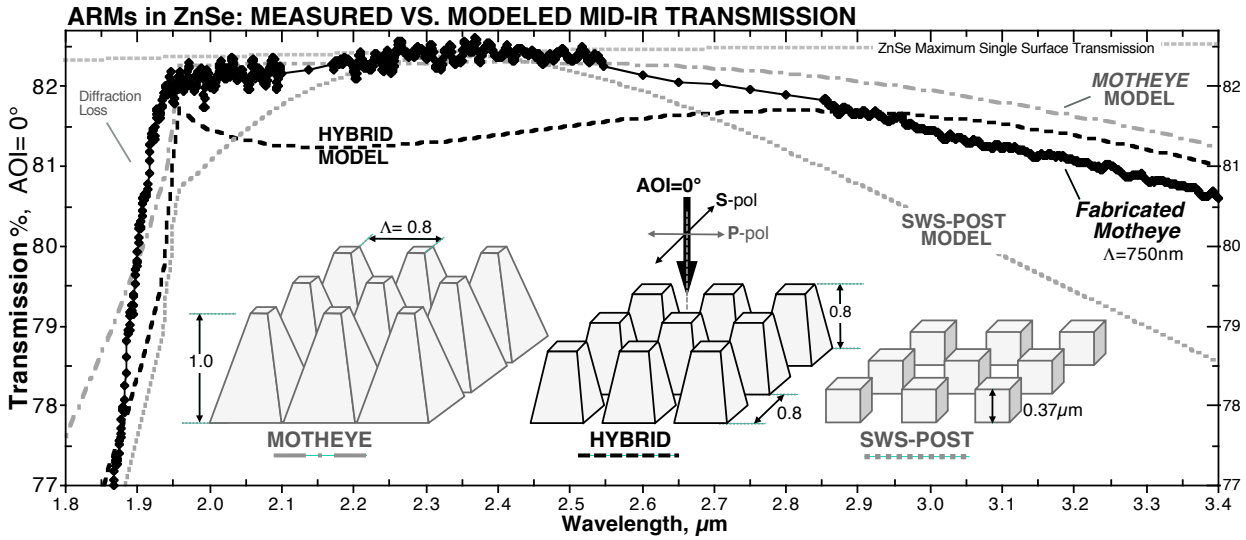

Figure 3: Measured transmission of Motheye ARMs textured ZnSe windows compared with the predicted transmission. Three types of ARMs texture designs were simulated with feature dimensions as shown.

3.0 ARMs FABRICATION AND MEASURED PERFORMANCE

Fabricating the array of pyramid features that make up a Motheye texture requires a lithographic step to originate the pattern followed by an etch step to transfer the pattern into the bulk material. Figure 4 illustrates the sequence whereby an original photo-pattern is produced in a sacrificial material (steps 1-3), and reactive ion etching (RIE), or the purely physical ion beam milling (IBM) methods are employed to transfer the patterns into the surface of the optic (steps 4-5). The process begins with coating the optic with a photosensitive polymer material, typically a positive photoresist common to the semiconductor industry (Step 1). Next, the non-contact and maskless interference lithography[9] (IL) technique is employed to expose a latent image of the Motheye texture in the sacrificial photoresist layer (Step 2). The structure lithography is completed by a wet development step that delineates the image as a surface relief texture (Step 3). After IBM or RIE plasma etching (Step 4), removal of the residual photoresist mask material completes the (Step 5) yielding a single material optic with an integrated AR function that is as robust and reliable as the bulk material. [This is in contrast to traditional AR coatings that require the deposition of multiple dissimilar thin film material layers, each layer with its own absorption, adhesion, and long-term survivability concerns.]

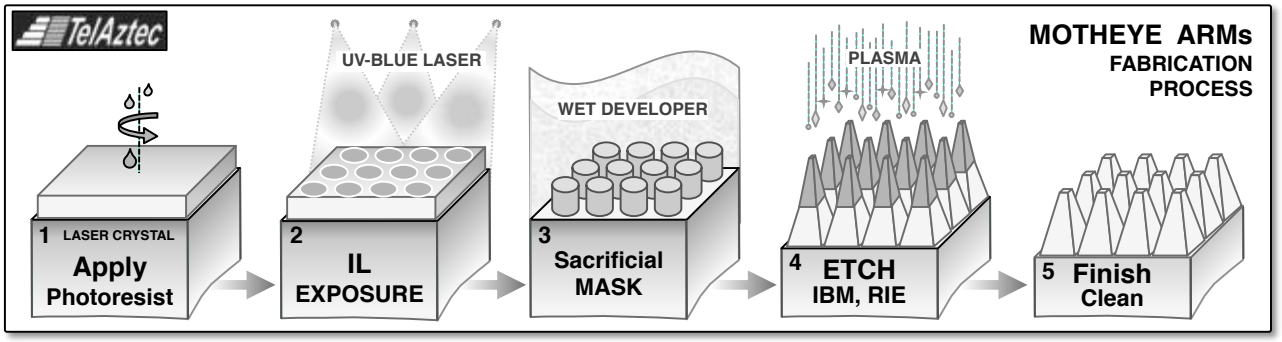

Figure 4: Process flow diagram for the fabrication of Motheye ARMs in ZnSe and ZnS materials.

Advantages of IL include the ability to produce feature sizes in the sub-100nm range, large pattern field sizes of 6" diameter or larger in a single exposure; huge depth of focus that allows the patterning of curved optics; and elimination of expensive photomasks and reticles needed with traditional lithography methods. The flexibility of the IL exposure system also allows for patterning irregular shape substrates, or multiple small area surfaces such as the end facets of Cr^{2+}:ZnSe laser gain media described herein. Motheye patterns are best produced with an IL system configured with two or three interfering beams. For a two-beam configuration, two exposures are made with a 90-degree substrate rotation between exposures to define posts with a four-fold symmetry. Figure 5 shows SEM images of a photoresist layer on ZnSe consisting of a checkerboard pattern of 610nm high posts arrayed on a 740nm grid as defined by double exposure two-beam IL. A higher contrast, single exposure using three overlapping beams produces a hexagonal array of posts with six-fold symmetry, a method that was preferred for the majority of this work.

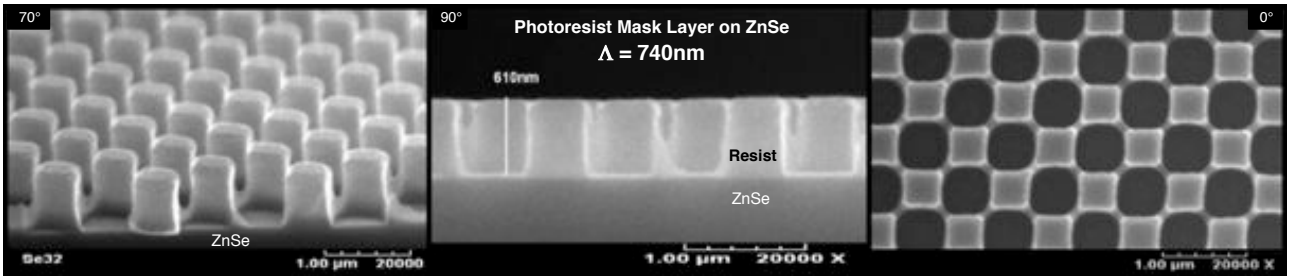

Figure 5: Elevation (70°), profile (90°), and overhead (0°) SEMs of 0.61µm high resist posts on ZnSe before RIE.

Transferring photoresist patterns into ZnS and ZnSe substrates with either RIE or IBM has historically been problematic due to the polycrystalline nature of the materials. A polished surface of a ZnS/ZnSe optic intersects thousands of grains of randomly oriented crystals, with each exposed crystal face having a different reactive volatility with respect to the plasma and/or impacting ions. As a result, the degree of etching varies from grain to grain, leaving a surface with ARMs structures varying in height and correspondingly, with a localized variation in optical performance. Figure 6 shows a square grid Motheye texture that was transferred into ZnSe with IBM of the photoresist pattern shown in Figure 5. The cone-type structures shown in the image are within a single grain intersecting the optical surface; however, in neighboring grains fractions of a millimeter away, the ARMs are etched to different depths. It is believed that the surface discontinuities exposed at the grain boundaries by the etching process lead directly to lower laser damage thresholds as further discussed in the laser damage testing section below.

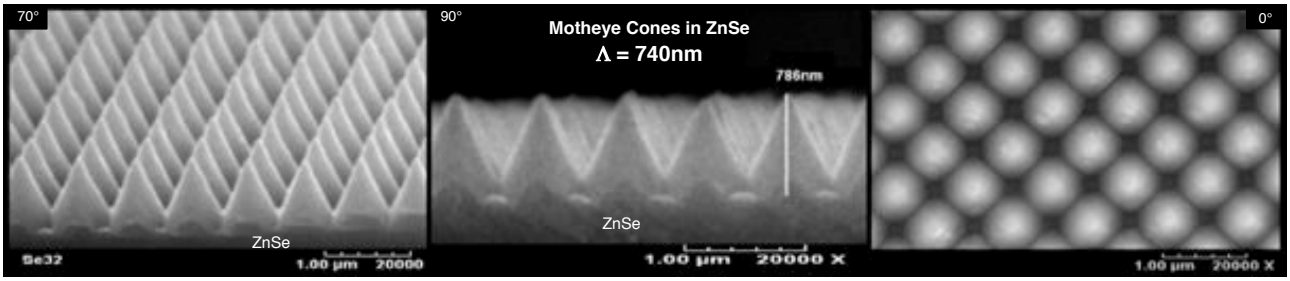

Figure 6: Elevation (70°), profile (90°), and overhead (0°) SEMs of 0.79µm high Motheye cones etched in ZnSe.

The grain boundary problem is illustrated in Figure 7 where low (200X) and high (400X) magnification SEMs are shown of an ARMs-treated ZnSe surface fabricated using IBM (note that conventional RIE methods produce the same result as IBM). The magnified image on the right of the darker triangle-shaped patch (indicated by the white rectangle) clearly shows the effect of varying etch rates across the grains. The Motheye textures around the perimeter of the triangular grain show the desired full height and fill-factor cones, while the cones within the triangular grain have been over etched, leaving shallow cones isolated on a planar background. More importantly, there are abrupt discontinuities observed on the three sides of the grain that are large enough to scatter light, reducing the laser damage resistance.

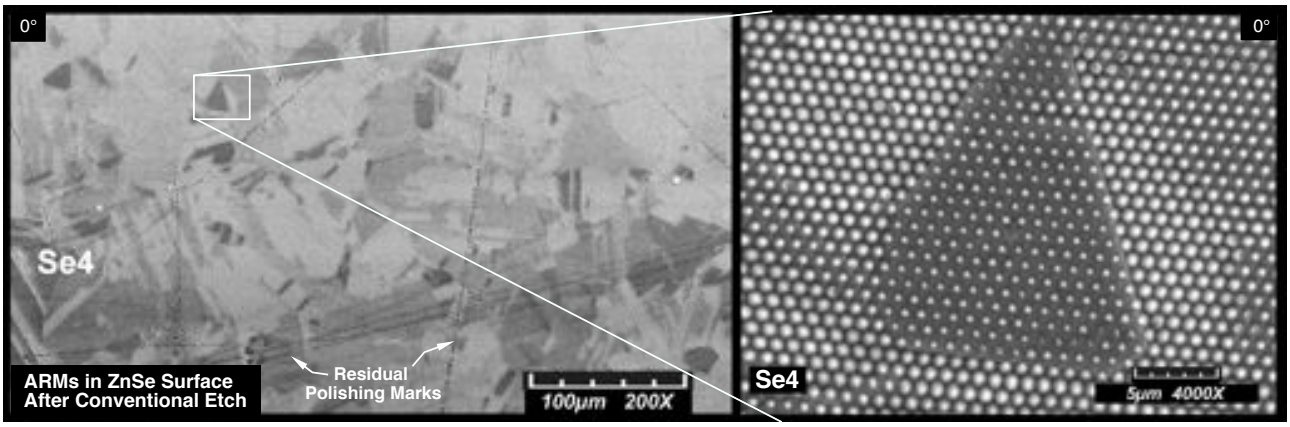

***Figure 7: ZnSe surface after ARMs fabrication using conventional etch processes; 200X magnification** (left) **and 4000X** (right).*

To address this issue, a new plasma RIE chemistry and process specific to II-VI materials, was developed to yield consistent reactant volatility during etching regardless of grain orientation, effectively eliminating the deleterious effects of polycrystalline grain boundary delineation. The results of the new grain-less etch process for ZnSe are shown in Figure 8, again represented by low (100X) and high (4000X) magnification optical and SEM images. No grain boundary definition is observed, and the high magnification image shows a uniform field of full height and full fill factor cones. The functional improvement seen with etching uniform AR textures includes higher transmission, no scattered light loss, and significantly higher pulsed laser damage resistance, as further discussed in the laser damage testing section below.

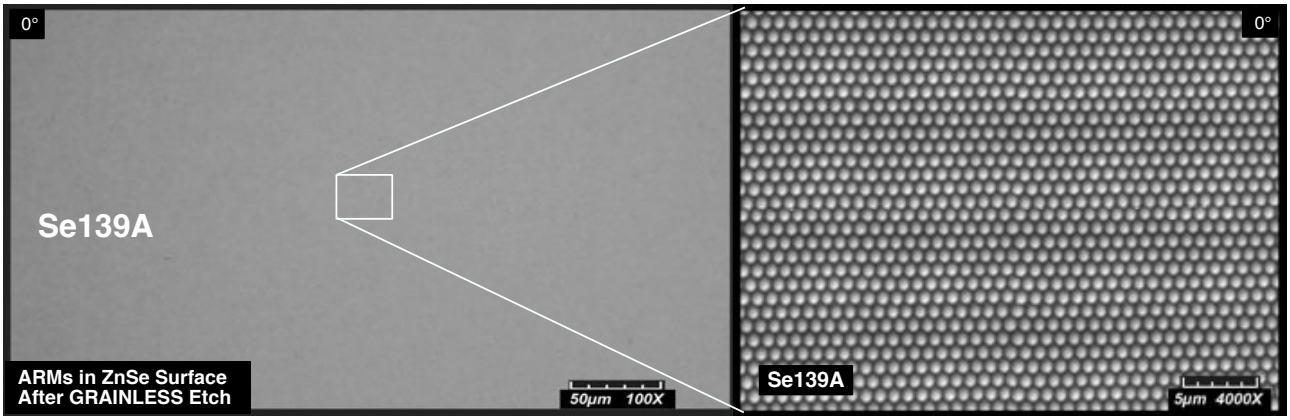

***Figure 8: ZnSe surface after ARMs fabrication using a new grain-less etch method; 100X magnification** (left) **and 4000X** (right).*

Clear ZnS, or ClearTran™ windows were also patterned and etched using the same grain-less RIE parameters developed for the ZnSe etching. IPG Photonics has described the potential advantages of using ZnS in place of ZnSe in their laser applications due to factors such as smaller polycrystalline grain size, higher laser damage resistance, and reduced susceptibility to thermal lensing effects (lower $^{dn}/_{dt}$). Similar to ZnSe, ClearTran suffers from the grain boundary definition issue as illustrated by the mosaic pattern resulting from standard etch processes shown in left image of Figure 9. The center and right images show low (100X) and high (4000X) magnification SEMs of the ClearTran surface after the new grain-less etch process, with a uniform field of Motheye cones similar to the ZnSe results.

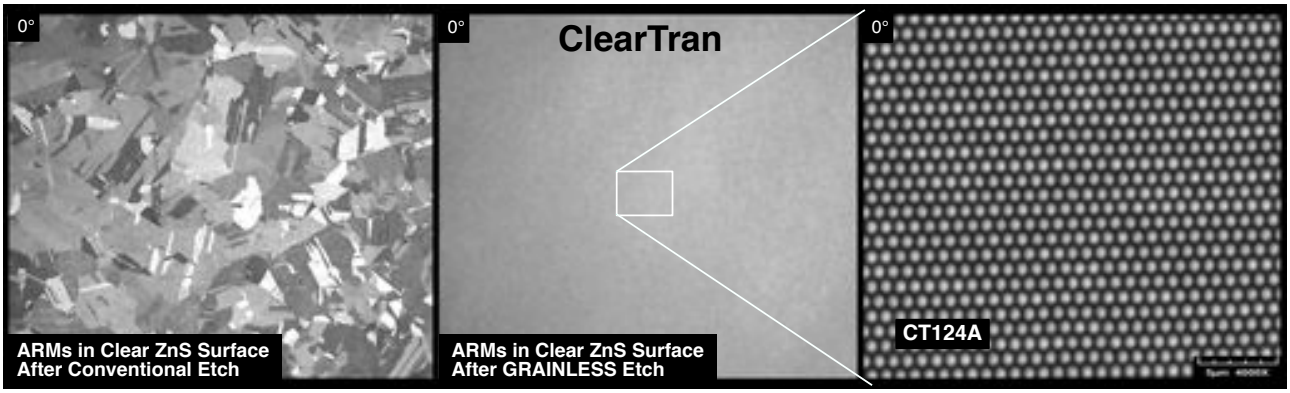

***Figure 9: Clear ZnS with ARMs etched in a conventional process** (left) **and the grainless method; 100X** (center)**, 4000X** (right).*

3.1. Motheye ARMs in ZnSe: Transmission Measurements

ARMs textures consisting of honeycomb arrays of cone structures like those shown in Figure 2 were fabricated in one surface of multiple ZnSe windows using IL and RIE processes. For a lossless single surface AR treatment in ZnSe, an 82.5% transmission level is expected over the mid-IR spectral range of from 1.9µm to 3.4µm, a range that corresponds to the pump and tuning bands of Cr^{2+}:ZnSe lasers. To date an average transmission of 81.3% has been achieved in multiple ARMs-treated ZnSe windows.

Figure 10 shows normal incidence transmission measurements of four ZnSe windows with ARMs fabricated in one surface recorded using an FTIR spectrophotometer. ZnSe window number Se144 consisting of a hexagonal array of 1100nm high cones like that shown in Figure 2, is indicated by the solid grey triangle markers and exhibits an average transmission of 81.3% over the wavelength range of 1.94 to 3.4µm in the mid-IR. Three other ARMs-treated windows are plotted with open circle markers (Se145), a black dotted curve (Se136), and solid grey circle markers (Se033). Of note in the plot, the transmission is identical for windows Se144, Se145, and Se136 over the range of from 1.9-2.2 µm – in particular at the 2.1µm wavelength used for the pulsed laser damage testing - with varying amounts of transmission roll off for Se145, Se136 and Se033 as the wavelength increases. The roll off is consistent with the gradient index function; the shallower Motheye structures noted in the plot legend for Se145 and Se136 result in reduced performance at longer wavelengths, due to less index grading as their height becomes a smaller fraction of the wavelength. Sample Se033, produced by IBM, exhibits reduced performance due to scattered light loss from the grain boundaries and the non-uniform feature size, as well as a lower cone height of only 790nm and a greater proportion of flat topology in the valleys between the cones.

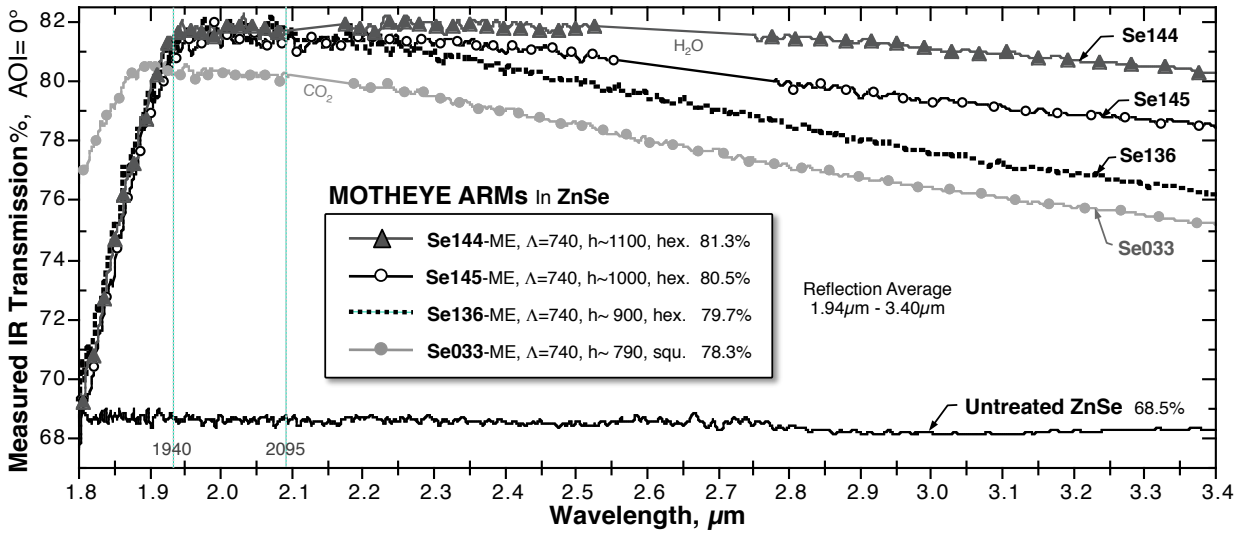

Figure 10: Measured transmission of ARMs-treated ZnSe windows with an improved polish and optimized RIE process

3.2. Motheye ARMs in Clear ZnS: Transmission Measurements

Several clear ZnS, windows were patterned with IL and etched using the same grain-less RIE process developed for ZnSe. Because clear ZnS material etches slower than ZnSe, the IL process was further optimized to increase the thickness of the photoresist mask layer so that it would survive longer in the etch plasma. Three-beam IL yielding the honeycomb array of cylindrical posts needed is the best choice for producing high aspect ratio features in photoresist as illustrated in the top row of SEM images in Figure 11. Photoresist posts about 1.1µm high are shown defined on the surface of a clear ZnS substrate. The lower row of SEMs in Figure 11 show the resulting array of cones after grain-less plasma etching through the sacrificial photoresist mask. The cones have become somewhat isolated and have a variable height around 650nm. This result indicates that the etch process continued for a time after the cones reached their maximum height, an over-etch that leads to the reduced height and has a negative impact on performance.

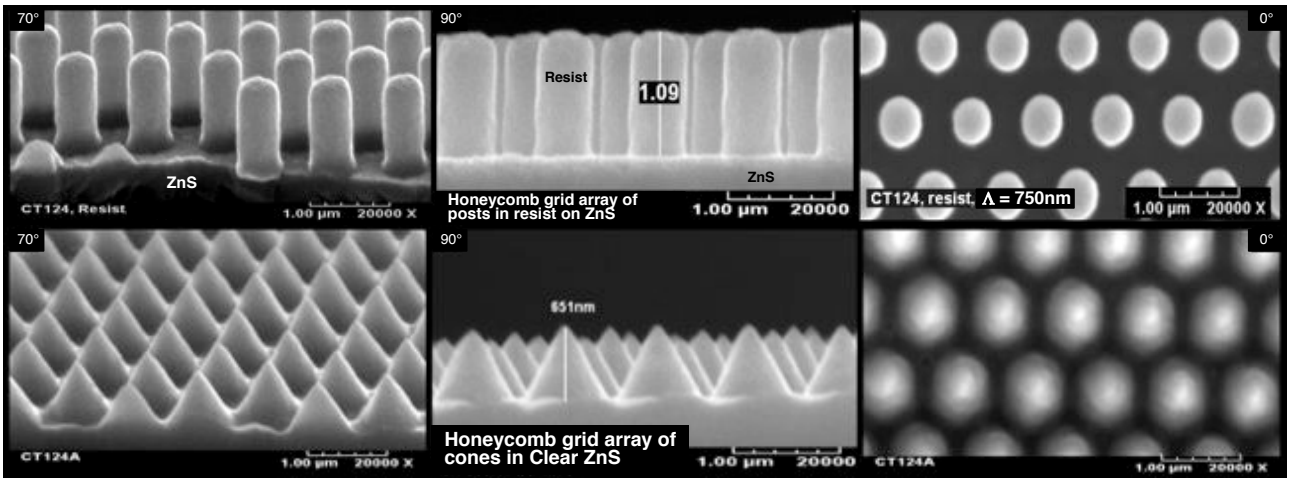

Figure 11: Top- Elevation** (70°), **Profile** (90°), **and Overhead** (0°) **SEMs of 1.1µm high resist posts on clear ZnS before RIE. Bottom- Elevation** (70°), **Profile** (90°), **and Overhead** (0°) **SEMs of cones etched in clear ZnS using the grain-less process.

Figure 12 shows the measured mid-IR transmission through two ARMs-treated clear ZnS windows over the pump and tuning bands of Cr^{2+}:ZnS (1.75µm to 3.4µm). The on-axis single surface reflection loss for Clear ZnS is calculated as $[n-1/n+1]^2$ where n is the refractive index, a value of 2.26 over the mid-IR spectral range. Eliminating all reflection losses from one surface would yield a maximum transmission of 84.5% through a planar ZnS window, and therefore the upper limit of the plot was set to that value. Neglecting absorption and scattering in the bulk and considering multiple internal reflections, transmission through an untreated window is expected to average 74% $[=2n/(n^2+1)]$ over the 1.94 to 3.4µm range, a level that is about 1% higher than the measured curve (solid black line). Sample CT124A, etched first with the insufficient height as shown in Figure 11, shows an average transmission near 77% as indicated by the grey curve with solid grey circle markers. Sample CT125 (dotted black curve) had greater depth cones and exhibits a higher average transmission of 79.1%. With further trials to improve the cone height and fill factor, an average transmission close to the maximum can be expected – similar to that attained after ZnSe ARMs process optimization.

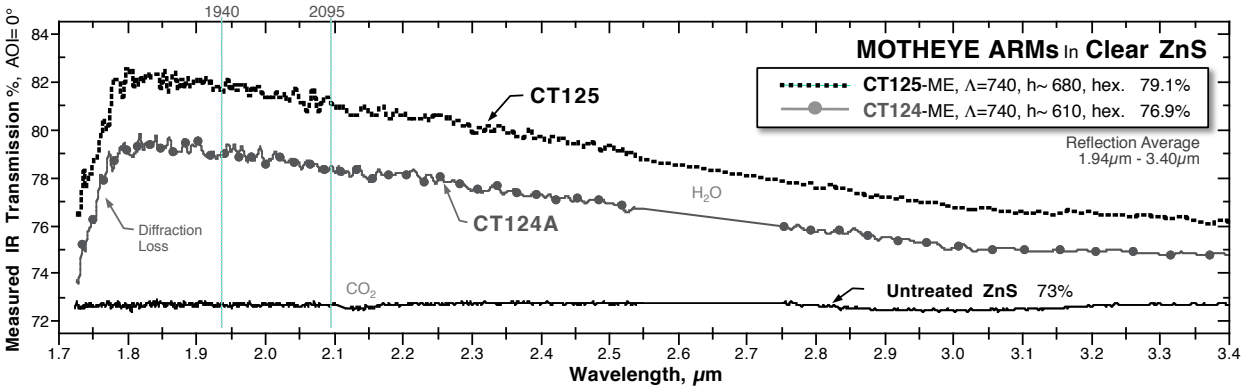

Figure 12: Measured transmission of ARMs-treated Clear ZnS windows fabricated with the grain-less RIE process.

3.3. Motheye ARMs in Cr^{2+}:ZnSe: Transmission Measurements

In SBIR work sponsored by the Air Force Research Laboratory and in collaboration with IPG Photonics, Motheye ARMs textures are being developed for Cr^{2+}:ZnSe laser gain media. Long thin slabs of ZnSe (7mm wide, 50mm long, 3.5mm thick, purchased from II-VI Inc.) were diffusion doped with chromium by IPG to a concentration near $6x10^{18}$ ions/cm^3. These slabs were diced into 7.5x7.5mm square sections and polished on both faces prior to starting the ARMs fabrication process. Figure 13 shows the infrared transmission of these Cr^{2+}:ZnSe windows (black circle markers, black line) compared to un-doped ZnSe (black curve), un-doped clear ZnS (grey curve), and samples of chromium doped ZnS (open circle markers, grey line) with a slightly lower concentration of chromium ions. Wide absorption bands for chromium are seen centered at 1.7µm and 1.8µm respectively for Cr^{2+}:ZnS and Cr^{2+}:ZnSe.

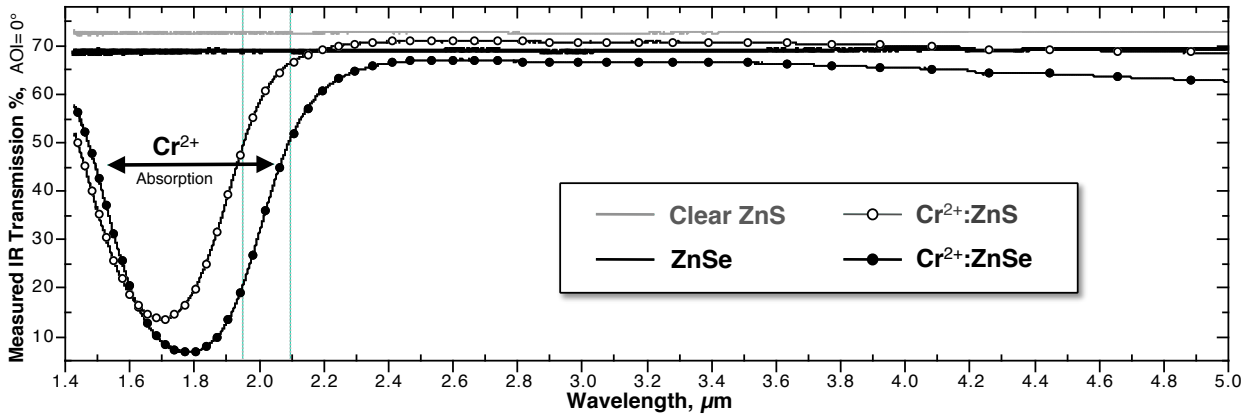

Figure 13: Mid-IR transmission of untreated ZnSe and clear ZnS compared to chromium doped ZnSe and ZnS windows.

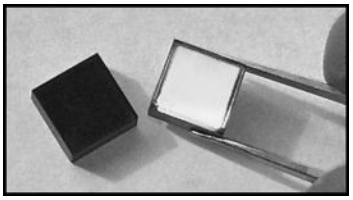

As described above, IL and the grain-less plasma etch recipe were used to fabricate ARMs textures in multiple windows for use in the pulsed and continuous wave laser damage testing described below. The image on the right shows a dark untreated Cr^{2+}:ZnSe crystal next to a Motheye textured crystal being held by tweezers at an angle to demonstrate the texture uniformity observed from the visible light diffraction. Figure 14 gives a plot of the measured mid-IR transmission of the two crystals showing a 9-10% increase in transmission for the Motheye textured crystal that is nearly constant across the band. SEM images of identically processed Motheye textured crystal number SeC13, shows truncated pyramids with a height of just 70% of the target depth. Further process refinement specific to the small laser crystal dimension is underway and expected to yield the >1µm high cones proven effective for un-doped ZnSe.

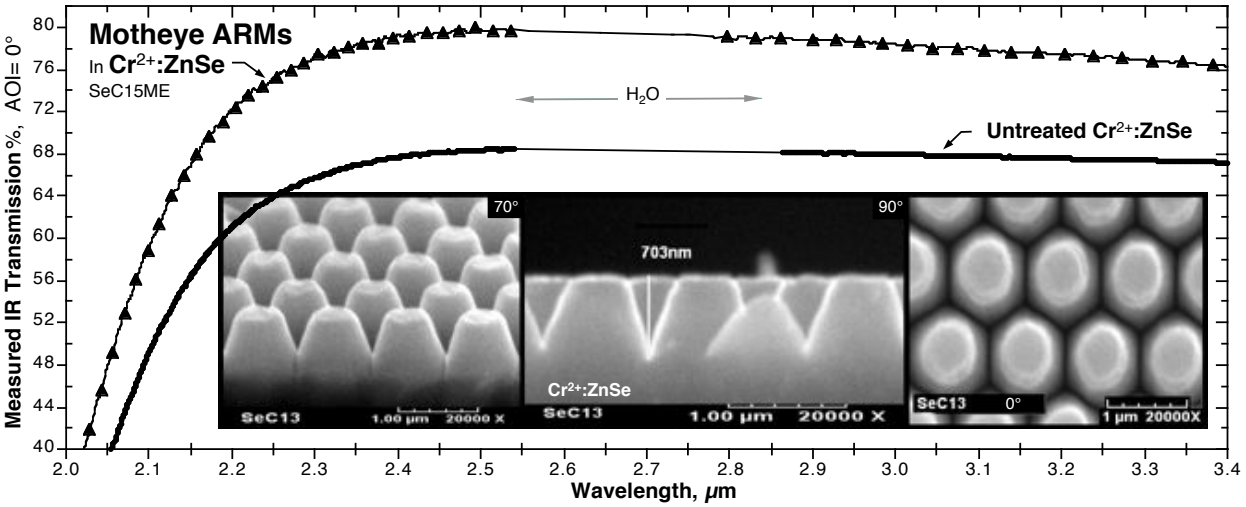

Figure 14: Transmission of untreated & ARMs-treated Cr^{2+}:ZnSe windows. *Inset:* ***SEMs of ARMs in Cr^{2+}:ZnSe sample SeC13.***

4.0 PULSED LASER DAMAGE TESTING

Following ISO 11254 standards for laser induced damage threshold (LiDT) testing, SPICA Technologies of Hollis New Hampshire conducted s-on-1 pulsed LiDT testing of untreated (polished) and ARMs treated samples of both ZnSe and Cr^{2+}:ZnSe. Using a 2.095µm wavelength Ho:YAG laser configured for an 80ns pulse width, 2Hz rep rate SPICA exposed between 35 and 60 sites on each sample to one of as many as 12 fluence levels. Up to 200 pulses were delivered at each exposure site as defined by a calibrated Gaussian beam (TEM_{00}) size in the range of 0.17-0.25mm. Other beam parameters were multiple longitudinal modes, random polarization state, and near normal incidence. SPICA determines the damage threshold using the "Least Fluence Failure" method, meaning the fluence level immediately preceding the level that causes permanent surface damage. Observation of damage is accomplished through increased scattering of a red He-Ne laser beam, plasma generation, and microscopic imaging of the exposure site using a Nomarski configured microscope at a magnification of 150 times normal size.

Twelve samples were prepared for the SPICA tests consisting of 8 ZnSe windows each 1-inch round by 2mm thick polished both surfaces, and 4 Cr^{2+}:ZnSe windows each 7.5x7.5mm square, 3.2mm thick also polished both sides. Two polish levels were examined, designated polish A or polish B, where polish A represents a simple commercial inspection polish level with no specification but likely resulting in a 60-40 scratch-dig, 5 waves flat surface, and polish B was completed by Opticraft of Woburn Massachusetts to a specification of 40-20 Scratch-Dig, 1-2 waves. The two polish levels were included to establish the expected correlation between damage threshold and polish level[22], and to observe the potential for the ARMs etch process to improve damage resistance through partial removal of residual polishing defects.

Figure 15 plots the damage frequency data collected by SPICA for some of the B-polish samples as a as a function of fluence level in both material categories, ZnSe and Cr^{2+}:ZnSe. Very high damage thresholds of 17.5 J/cm^2 and 14.0 J/cm^2 are found for the ZnSe untreated (open cross markers, dotted grey line) and ARMs-treated (open triangle markers, solid grey line) samples respectively. These LiDT levels are higher than the approximately 2 J/cm^2 often found in the literature[23]. This fact may be due to the longer pulse length and low repetition rate of the laser used for the test, however, comparison of the 12 variants all exposed with the same parameters yields useful information. As with prior damage testing in several other materials, the ARMs-treated ZnSe thresholds are found to be comparable to the untreated ZnSe surfaces. Results for the Cr^{2+}:ZnSe samples also show high thresholds of 8.5 J/cm^2 and 7.0 J/cm^2 for untreated (solid grey cross markers, dotted grey line) and ARMs-treated (black triangle markers, black line) Cr^{2+}:ZnSe samples respectively. Again the untreated and ARMs treated thresholds are nearly equivalent, but at half the level of the un-doped ZnSe, a result that is likely due to the increased absorption of the chromium ions at 2095nm.

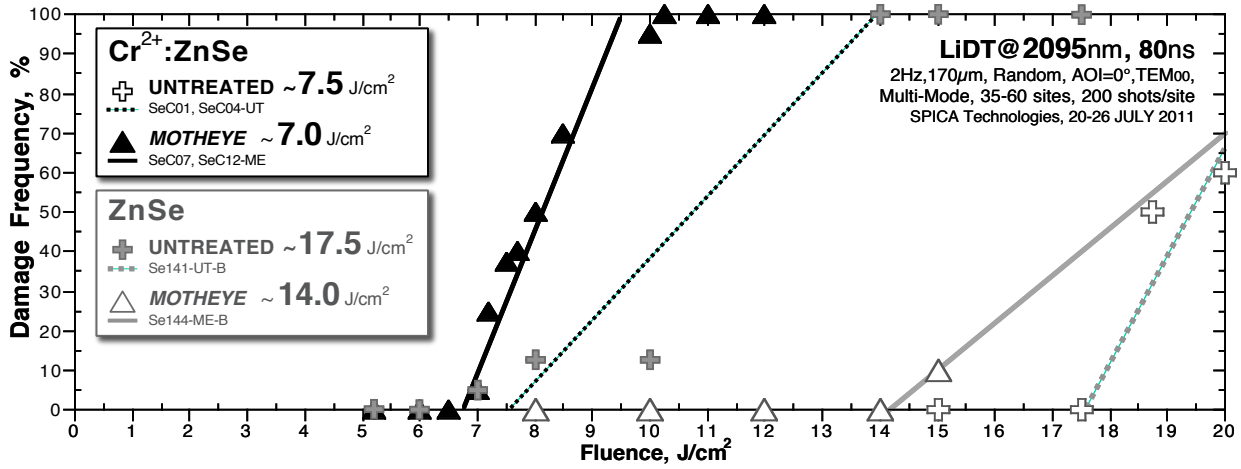

Figure 15: Damage frequency vs. fluence plot for untreated and ARMs-treated ZnSe and Cr^{2+}:ZnSe.

Further detail comparing all the damage testing results of this study is given by the bar chart of Figure 16. The ZnSe sample results are arranged in three groups isolating process parameters such as the initial polish level and the type of ARMs fabrication (ion milling IBM, or the new grain-less RIE). The first group consists of one untreated (UT) and one ARMs-treated (ME) ZnSe window each with the low grade A-polish where the Motheye texture was generated by IBM, a conventional physical etch process that reveals polycrystalline grain boundaries as described above in Figures 7 & 9.

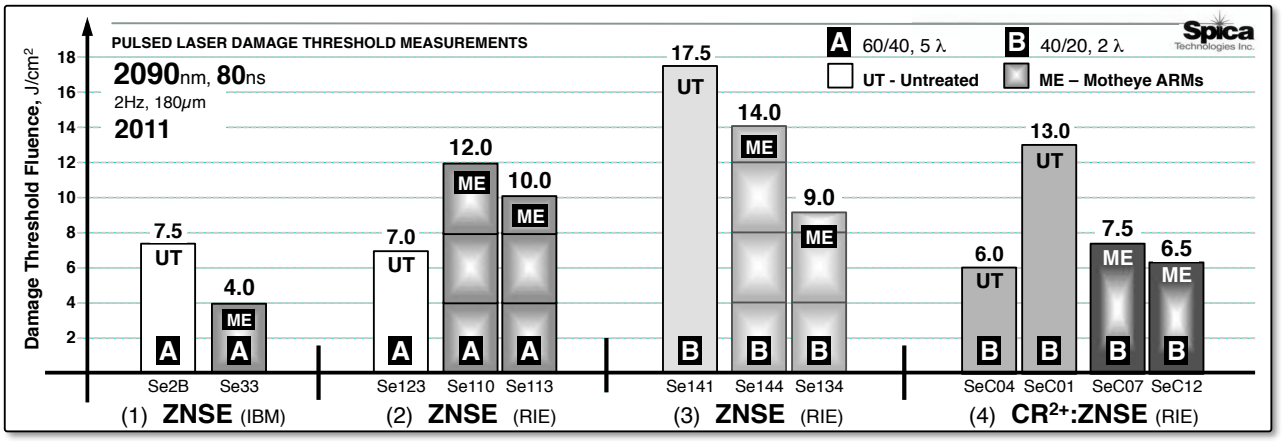

Figure 16: Bar chart of the pulsed LiDT for all untreated and ARMs-treated ZnSe and Cr^{2+}:ZnSe windows tested.

Comparing the first group with the second group of three samples that also were prepared with the A-polish, the untreated samples are found to have similar thresholds as expected near 7.0 J/cm^2, but the second group Motheye texture samples fabricated using the new grain-less process show damage thresholds of 12 and 10 J/cm^2, more than 50% higher than the untreated samples and three times the level of the IBM processed sample. Based on prior testing[20] with this SPICA system comparing the untreated, ARMs-treated, and thin-film AR coated materials CdZnTe, As_2S_3, zinc germanium phosphide (ZnGeP2), and gallium arsenide (GaAs), it is likely that the group two Motheye samples have damage thresholds at least three times that of any comparable performance thin-film AR coating design.

Damage thresholds were increased further through the combination of the new grain-less ARMs etch process with the higher grade B-polish as indicated by the third test group – in particular the untreated sample Se141 with a threshold 2.5 times higher than the untreated A-polish samples of groups 1 and 2. The two B-polish Motheye samples in the third group have an average damage threshold that is slightly higher than the average threshold for the group two A-polish samples, indicating that further gains might be achieved through improved ARMs texture processing. Both the group two and three, and even the group four Cr^{2+}:ZnSe Motheye sample data validate the concept that the new grain-less ARMs fabrication process is effective for increasing damage resistance. In essence, the new RIE process is removing a significant portion of residual sub-surface polish damage, surface defects and contamination as illustrated in the diagrams of Figure 17. On the left in the figure a cross section of a three-layer thin-film AR coating stack is shown deposited over a representation of the polycrystalline grain structure of ZnSe where different crystal orientations are indicated by the hash lines, and a grey line delineates the boundary between different crystal orientations. Depending on the complexity of the thin-film stack, surface defects and contaminants will be partially replicated in the external film surface. Heavy irregular black lines represent sub-surface cracks and defects produced by even the lightest pressure polishing methods, defects that significantly reduce damage resistance and can only be partially mitigated by thin-film coatings. The center diagram shows the same ZnSe cross-section after fabricating an array of Motheye-type pyramids using a conventional etch process. Most surface pits, scratches and oxides will be removed along with a significant portion of the sub-surface polish damage. However, the different crystal orientations will etch at different

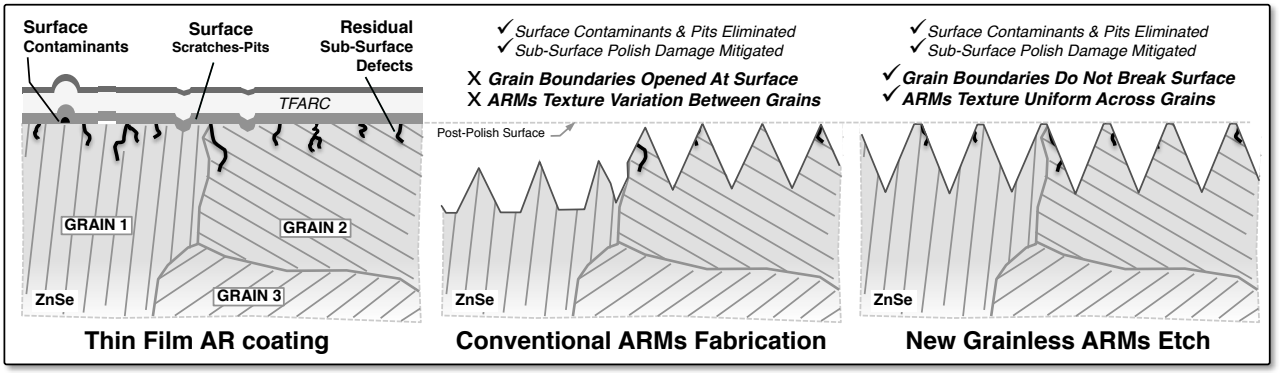

***Figure 17: ZnSe AR concept diagrams, thin film ARCs** (left), **standard process ARMs** (center), **grain-less process ARMs** (right).*

rates leading to a revelation of the grain boundaries at the surface and a wide variation in the pyramid dimensions from grain to grain – yielding a net negative impact on damage resistance as indicated by the group 1 test data. The new grain-less process removes these limitations and etches ZnSe uniformly across different crystal grains as illustrated in the right most diagram in Figure 17. Such uniformity reduces scattered light, mitigates polishing damage, and removes surface contaminants that combined significantly improve laser damage resistance as indicated by the group 3 & 4 data.

The concept of removing residual polishing defects as a means of increasing LiDT is not new; thermal annealing and wet etching after super-polish, are known to improve the LiDT of fused silica optics[24-27]. However, polycrystalline ZnSe and ZnS cannot be thermally annealed like glasses, and an isotropic wet etching process produces the undesirable grain boundary definition just described. Extending the concept of damage precursor removal during etching, a "Plasma Surface Polish", or PSP concept is under development as an effective post-polish damage mitigation process. Using the same plasma chemistry that yields grain boundary defect free ARMs textures, a blanket etch to remove surface material after polishing may effectively eliminate all surface and sub-surface defects. The PSP etch depth may only need to be in the 1-5µm range to smooth out all damage in a manner similar to that employed for epitaxial growth on ZnSe for LEDs[28]. Fabricating ARMs after the PSP treatment would leave a defect free texture as illustrated in the diagram on the right. An effort to test this concept with more extensive damage testing is underway as part of an AFRL Phase 2 SBIR contract.

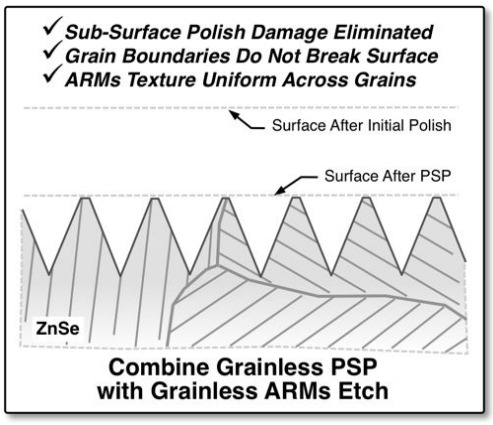

4.1 Pulsed LiDT Testing at **2095**nm, 80ns: Damage Site Analysis

SEM images of damage sites in ZnSe and Cr^{2+}:ZnSe were recorded in an effort to better understand the nature of the damage, and to correlate with the surface preparation issues described above. On the left in Figure 18 a damage site in the untreated, A-polish ZnSe sample number Se2B, shows a crater with a fused, or melted quality and a network of fine cracks that might correspond to the polycrystalline grain boundaries. Interestingly, point defects seem to form along these fine cracks and may serve to initiate damage. The damage to the Motheye textured surface of A-polish ZnSe sample Se33 shown on the right also appears to have a melted quality suggesting surface heating and reflow. At 2000X magnification, the cracks seen in the upper left corner of the Motheye surface image appear to be in the 10µm scale range which is at least four times smaller than the specified average grain size for ZnSe, indicating they may be the result of some other process such as rapid cooling. Similar cracks can be seen within the B-polish Motheye surface damage site shown in the lower right SEM image of Figure 19.

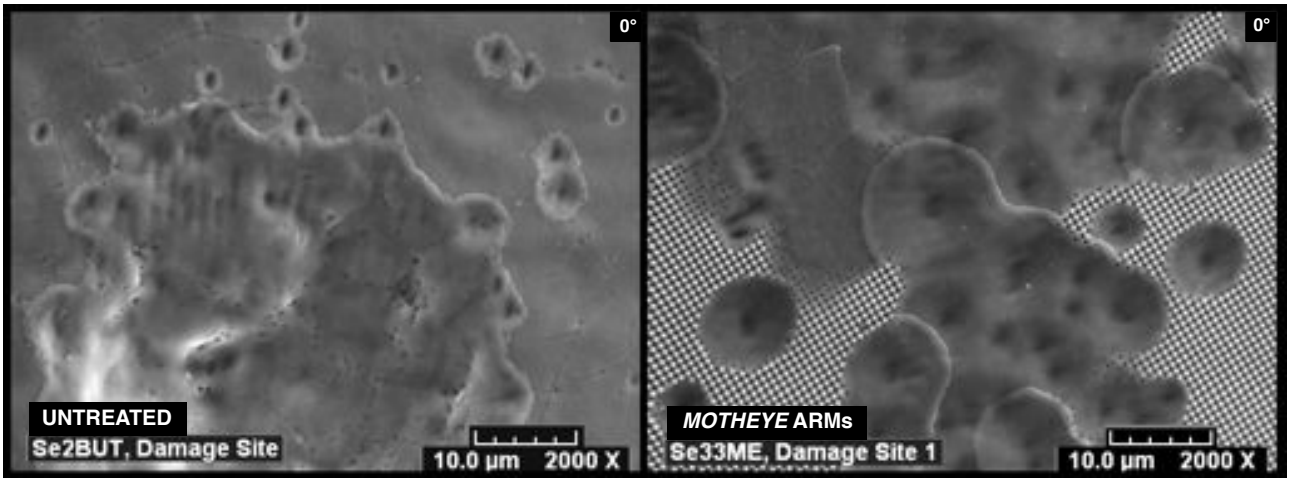

Figure 18: Overhead SEM views of laser induced damage sites in untreated** (left) **and Motheye ARMs treated** (right) **ZnSe.

Residual polishing marks left by the low grade A-polish can be seen in the untreated ZnSe sample surface damage site image in the upper left corner of Figure 19. A magnified image of this site is also given in the upper right of Figure 19 showing the detail of the area marked by the white circle. Again many small craters are distributed around what must be the central initiation point suggesting that debris ejected from the initial damage creates satellite damage pits.

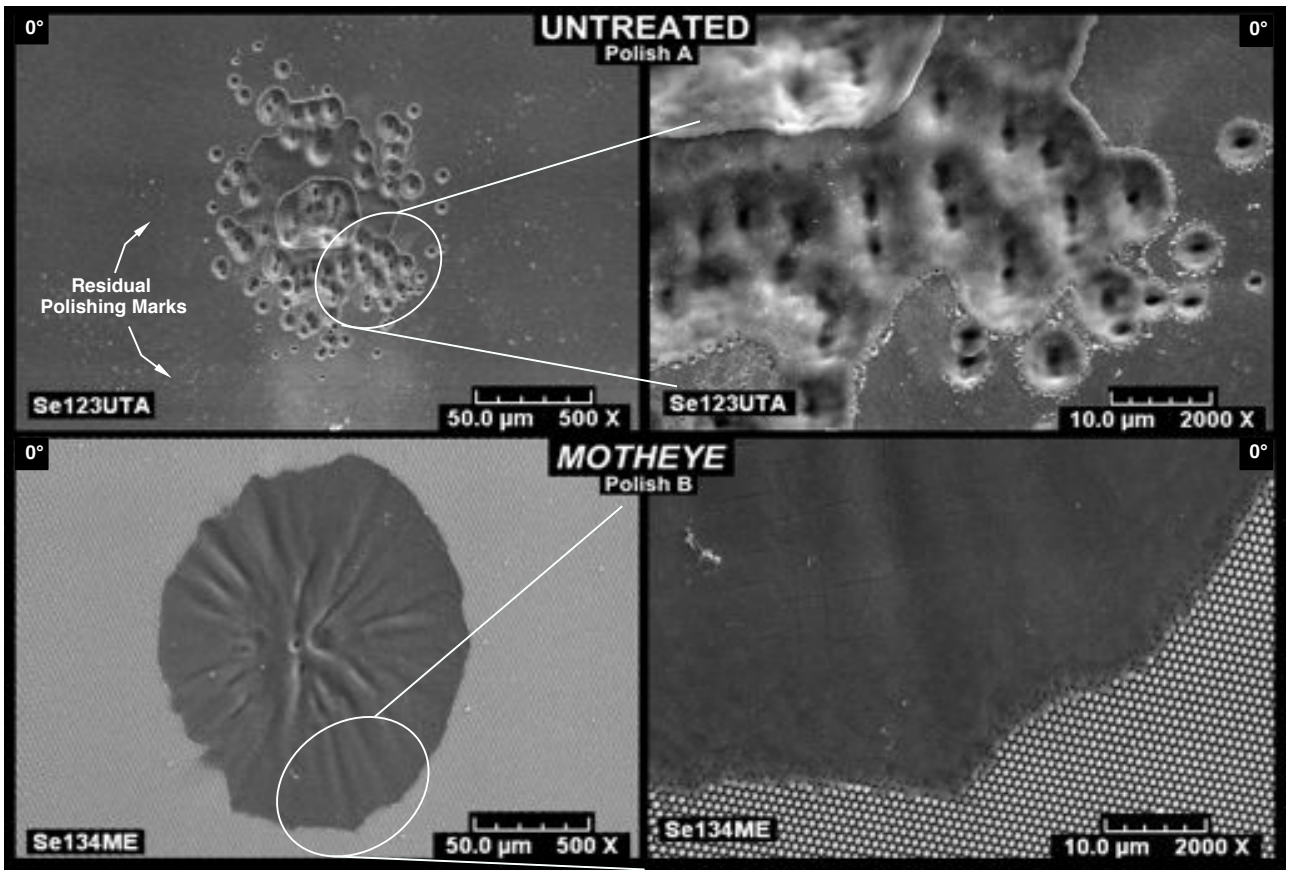

Figure 19: Overhead SEM views of laser induced damage sites in untreated** (top) **and Motheye ARMs treated** (bottom) **ZnSe.

The bottom row of images in Figure 19 show a damage site in a Motheye textured ZnSe surface prepared initially with the higher grade B-polish. Damage at this site is very shallow and uniform with depressions that radiate out from a central point. The magnified view of the area within the white circle shown in the lower right image shows a fused appearance that may only be as deep as the honeycomb array of cones.

Damage sites in the Cr^{2+}:ZnSe windows were typically much smaller than the sites found on the ZnSe surfaces as shown in Figure 20. This is likely a result of the lower energy exposures needed to define the threshold, energies that produce melt damage due to the chromium absorption, but not the collateral damage of surface material ejected due to cracking along grain boundaries seen at higher fluence levels. Even the largest craters like that shown for the untreated ZnSe sample on the left image of Figure 20, appear to have been rapidly melted with features and radial ejecta that are rounded and smooth as if in a liquid form.

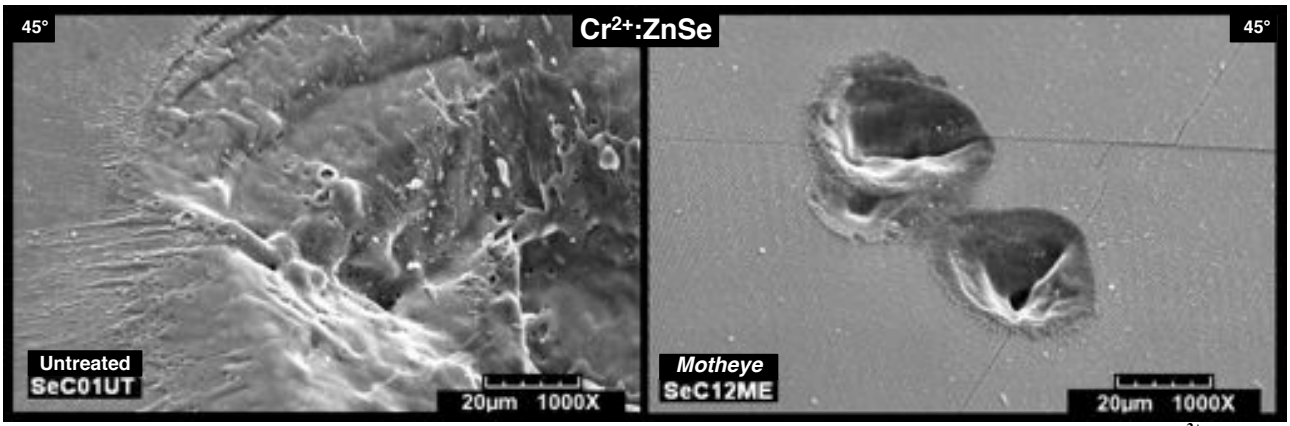

Figure 20: Elevation SEM views of laser induced damage sites in untreated** (left) **and Motheye ARMs treated** (right) **Cr^{2+}:ZnSe.

5.0 CONTINUOUS WAVE LASER DAMAGE TESTING

Continuous wave (CW) laser damage testing was conducted by IPG Photonics using a thulium fiber laser operating at a wavelength of 1.94µm, a convenient wavelength for pumping Cr^{2+}:ZnSe that is about half way between the absorption peak and the long-wave FWHM point of the wide chromium absorption band (See Figure 13 above). Three samples of Cr^{2+}:ZnSe with the B-polish consisting of one untreated and two ARMs treated, were subjected to a type of s-on-1 CW laser test. A lens focused the beam from the fiber laser onto the sample surface to a spot size of 80µm ($1/e^2$). Because of the heavy chromium absorption, each sample was fixed in a custom water-cooled copper heat sink to provide adequate heat removal. Detectors were located to record over time both the incident laser power and the power transmitted through each sample. The beam was scanned to 25 sites on each sample with each site being exposed to one of five power levels for 10 minutes, or until damage occurred as recorded by a sharp drop in transmitted power. This power drop would trigger a shutter to block the incident beam within a fraction of a second, a necessary step to avoid complete destruction of the sample from internal cracking. Figure 21 is a plot of the input and transmitted power over time for two of the 25 sites exposed on Motheye ARMs sample SeC16ME. The first site, Area 018, was undamaged after 10 minutes at an incident power of 18 Watts (black curve) and a transmitted power of 12 Watts (grey curve and triangle markers). At 20 Watts input – 13 Watts transmitted power, damage occurred in approximately 90 seconds at Area 019 as shown on the right in the figure. The ratio of transmitted to incident power for both Motheye samples was about 66%, dropping to 53% for the untreated sample, values that are consistent with the decreased Fresnel loss from the ARMs treated surface. A fixed magnification image of each exposure area was recorded to characterize the damage as shown in Figure 22. Photographs of each sample after testing are shown on the right above, where a network of internal fracturing can be seen originating from multiple surface sites.

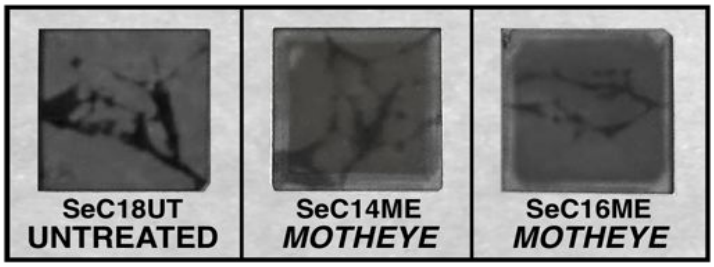

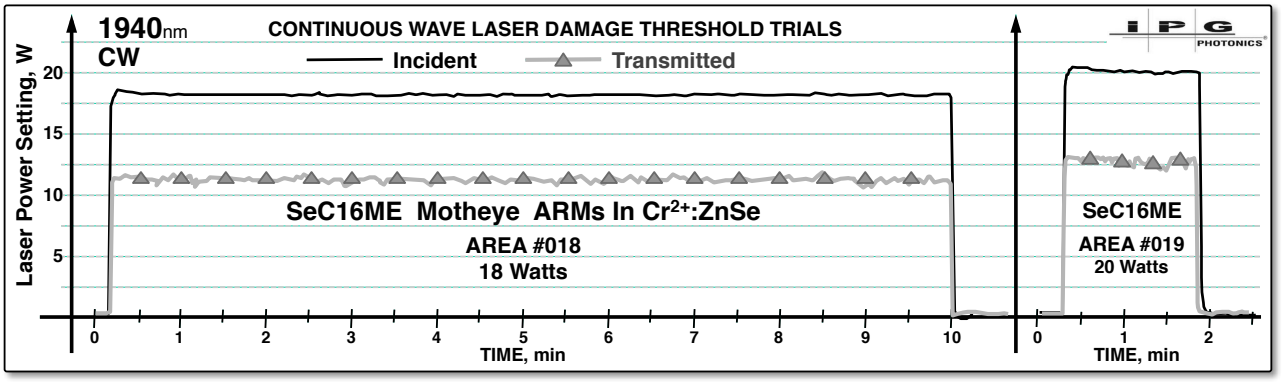

Figure 21: Input and transmitted power recorded during CW operation for power levels below & above the damage threshold.

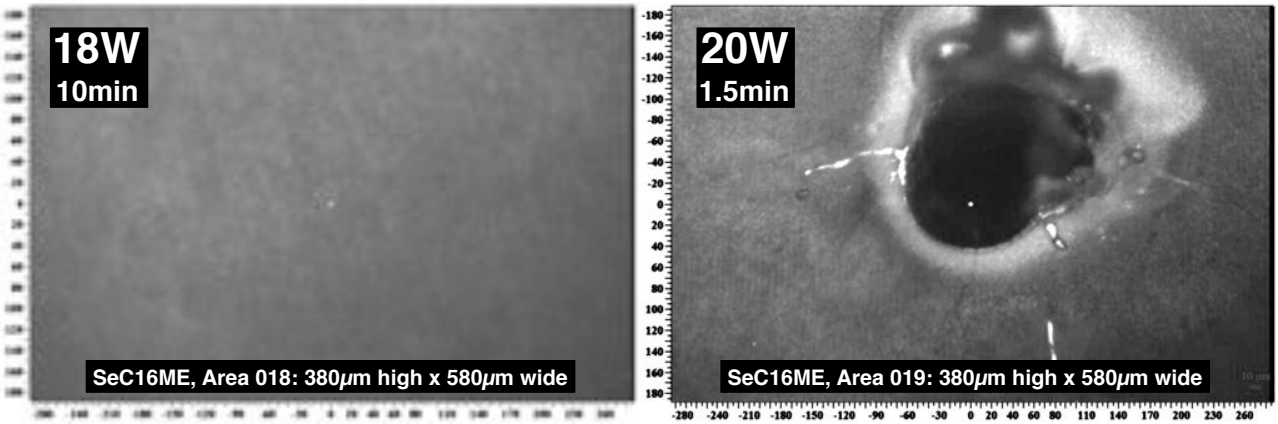

Figure 22: Images of the exposed surfaces for power levels below (left) & above (right) the CW damage threshold.

Figure 23 summarizes the CW damage testing results for all three samples showing the damage frequency as a function of the laser power setting. For the untreated sample SeC18UT (open cross markers, grey line), no damage was observed in 15 sites up to a power of 20W, an average intensity over the 80µm spot on the surface of 0.4 MW/cm^2. At 25W (0.5 MW/cm^2), damage occurred within 12-30 seconds at all five sites exposed, and at 30W (0.6MW/cm^2) all five sites damaged within 1-6 seconds. For Motheye samples SeC14ME (open triangle markers, thin black line) and SeC16ME (solid black triangle markers, thick black line), no damage was observed in 13-14 sites up to a power of 18W. One site was damaged on SeC16ME at 18W (20% fail). All sites on SeC14ME and SeC16ME failed within 30-120 seconds at 20W, and within 1-5 seconds at 25W. Considering the fact that Fresnel reflection loss has been eliminated by the ARMs textures in the expose surface of both SeC14ME and SeC16ME, about 17% more power will enter the bulk crystal. Adjusting the power absorbed by the bulk by 17% yields the data plotted as the grey diamonds with the dashed grey curve. Therefore, with regards to the optical damage threshold, this will put modified crystals in the same range with not modified crystals. *Both* survive power densities in the range of 0.4 to 0.5 MW/cm^2, a value significantly higher than thin-film AR coatings tested in a similar manner by IPG.

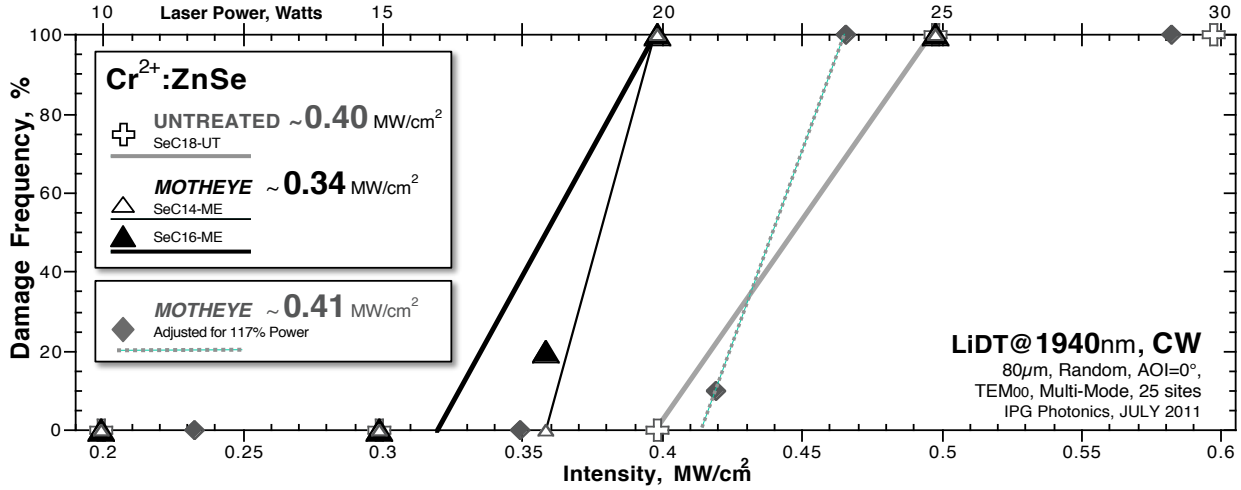

Figure 23: Damage frequency as a function of CW power for untreated and ARMs treated Cr^{2+}:ZnSe crystals tested at 1940nm.

6.0 SUMMARY

The development of AR microstructure technology for metal-ion doped ZnSe gain media as a replacement for thin film AR coatings is driven by the promising benefits of ARMs- superior power handling capability, wider bandwidth, elimination of water absorption concerns, and increased laser lifetime and reliability. Motheye ARMs textures were fabricated in ZnSe windows exhibiting reflection losses below 0.2% over a 1500nm wide spectral range in the mid-IR. ARMs were also demonstrated in chromium-ion doped ZnSe (Cr^{2+}:ZnSe) and ClearTran ZnS. In standardized pulsed laser induced damage threshold (LiDT) testing at a wavelength of 2.1µm, damage thresholds for ARMs treated Cr^{2+}:ZnSe and ZnSe windows were found to be three to seven times higher than the 2 J/cm^2 reported for thin-film AR coatings. Improving the quality of the initial surface polishing of both untreated and ARMs treated samples yielded a 2X increase in the measured LiDT. Continuous wave laser damage testing at a wavelength of 1.94µm conducted by IPG Photonics indicates that ARMs-treated Cr^{2+}:ZnSe windows can survive power densities up to 0.5 MW/cm^2, a level equivalent to untreated material and estimated to be significantly higher than the damage threshold of thin-film AR coated Cr^{2+}:ZnSe. Further studies are underway for refining a plasma-based post-polish subsurface damage mitigation process that, combined with the ARMs etch process shows potential for dramatically increasing the reliability of metal-ion doped laser crystals in mid-IR HEL systems.

7.0 ACKNOWLEDGEMENTS

The authors gratefully acknowledge the significant support of William D. Mitchell, Patrick A. Berry, and Dr. Kenneth Schepler of the Air Force Research Laboratory, Sensors Directorate, Wright-Patterson Air Force Base, through the SBIR program, contract # FA8650-12-C-1367 (AFRL PUBLICATION APPROVAL # 88ABW-2012-4222, 03AUG2012). The authors also thank Mike Thomas of SPICA Technologies for the detailed pulsed LiDT testing at 2095nm. SEM analysis of the ARMs textures and laser damage sites was performed by Mr. John Knowles at MicroVision Laboratories, Inc. in Chelmsford Massachusetts (http://www.microvisionlabs.com).

8.0 REFERENCES

[1] Sorokina, I.T., et.al., "Efficient broadly tunable continuous-wave Cr^{2+}:ZnSe laser," JOSA B, **18**, 7, 926 (2001)
[2] Mirov, S., et.al., "Recent progress in transition metal doped II-VI mid-IR lasers," Proc.SPIE **6552**, 65520Y (2007)
[3] Schepler, K., & Berry, P., "A promising mid-infrared transition metal ion laser," SPIE Newsroom, 22 May (2007)
[4] Moskalev, I.S., et.al., "Tunable, Single-Frequency, and Multi-Watt Continuous-Wave Cr^{2+}:ZnSe Lasers," Optics Express **16**, (2008)
[5] Voronov, A.A., et.al., "A continuous-wave Fe^{2+}:ZnSe laser," Quantum Electronics **38**, 1113-1116 (2008)
[6] Mirov, S., et.al., "Progress in Cr^{2+} and Fe^{2+} doped mid-IR laser materials," Laser & Photonics Review **4**, 21 (2010)
[7] Moskalev, I.S., Fedorov, V.V., and Mirov, S.B., "Tunable, Single-Frequency, and Multi-Watt Continuous-Wave Cr2+:ZnSe Lasers," Optics Express **16**, 4145-4153 (2008)
[8] Wilson, S.J., Hutley,M.C., "The optical properties of 'moth eye' antireflection surfaces," Optica Acta, **29,** 7 (1982)
[9] Hobbs, D.S., et. al., "Automated Interference Lithography Systems for Generation of Sub-Micron Feature Size Patterns," Proc. SPIE **3879**, 124 (1999)
[10] Hobbs, D.S., and MacLeod, B.D., "Design, Fabrication and Measured Performance of Anti-Reflecting Surface Textures in Infrared Transmitting Materials," Proc. SPIE **5786**, (2005)
[11] Hobbs, D.S., and MacLeod, B.D., "Update on the Development of High Performance Anti-Reflecting Surface Relief Micro-Structures," Proc. SPIE, Vol. **6545**, (2007)
[12] Hobbs, D.S., and MacLeod, B.D., "Long Life, High Performance Anti-Reflection Treatment for HgCdTe Infrared Focal Plane Arrays," Proc. SPIE **6940**, (2008)
[13] Hobbs, D.S., "Study of the Environmental and Optical Durability of AR Microstructures in Sapphire, ALON, and Diamond," Proc. SPIE **7302**, 73020J (2009)
[14] Cook, L.M., et.al., "Integral Antireflective Surface Production on Optical Glass," Journal of the American Ceramic Society **65**, 152 (1982)
[15] Lowdermilk, W.H. and Milam, D., "Graded-index antireflection surfaces for high-power laser applications," Applied Physics Letters **36**, 891 (1980)
[16] Hobbs, D.S., and MacLeod, B.D., "High Laser Damage Threshold Surface Relief Micro-Structures for Anti-Reflection Applications," Proc. SPIE **6720**, 67200L (2007)
[17] Hobbs, D.S., "Laser damage threshold measurements of anti-reflection microstructures operating in the near UV and mid-infrared," Proc. SPIE **7842**, 78421Z (2010)
[18] Hobbs, D.S., "Laser Damage Threshold Measurements of Microstructure-Based High Reflectors," Boulder Damage Symposium XL Proc. SPIE **7132**, (2008)
[19] Hobbs, D.S., et.al., "Laser damage resistant anti-reflection microstructures in Raytheon ceramic YAG, sapphire, ALON, and quartz," Proc. SPIE **8016**, 80160T (2011)
[20] MacLeod, B.D., Hobbs, D.S., and Sabatino, E. "Moldable AR microstructures for improved laser transmission and damage resistance in CIRCM fiber optic beam delivery systems," Proc. SPIE **8016**, 80160Q (2011)
[21] Du, Y.,et.al.,"Laser-induced damage properties of antireflective porous glasses," Proc. SPIE **8206**, 82060Q (2012)
[22] Krol, H., et.al., "Study of laser-induced damage at 2 microns on coated and uncoated ZnSe substrates," Proc. SPIE **6403**, 640316 (2007)
[23] Zawiliski, K.T., et.al., "Large aperture single crystal ZnGeP2 for high-energy applications," Journal of Crystal Growth **310**, 1891–1896 (2008)
[24] Shen, N., et.al., "Thermal annealing of laser damage precursors on fused silica surfaces," Opt. Eng. **51**, (2012)
[25] Stolz, C.J. et.al., "Engineering meter-scale laser resistant coatings for the near IR," Proc. SPIE **5963**, (2005)
[26] M. R. Borden, M.R., et.al., "Improved method for laser damage testing coated optics," Proc. SPIE **5991**, (2005)
[27] Krol, H., et.al., "LIDT improvement of multilayer coatings by accurate analysis of fabrication steps," Proc. SPIE **5963**, 596311 (2005)
[28] Hughes, W.C., et.al., "Surface preparation of ZnSe substrates for MBE growth of II-VI light emitters," Journal of Crystal Growth **176**, 546-551 (1997)